Innexin function dictates the spatial relationship between distal somatic cells in the *Caenorhabditis elegans* gonad without impacting the germline stem cell pool

Theadora Tolkin*[1], Ariz Mohammed*[2], Todd Starich[3], Tim Schedl[#,2], E. Jane Albert Hubbard[#,1,4,5], David Greenstein[#, 3]

[1] Kimmel Center for Biology and Medicine at the Skirball Institute, NYU Grossman School of Medicine, New York, NY, United States

[2] Department of Genetics, Washington University School of Medicine, St. Louis, MO, United States

[3] Department of Genetics, Cell Biology and Development, University of Minnesota, Minneapolis, MN, United States

[4] Department of Cell Biology, NYU Grossman School of Medicine, New York, NY, United States

[5] Department of Pathology, NYU Grossman School of Medicine, New York, NY, United States

*equal contribution

co-corresponding

Abstract

Gap-junctional signaling mediates myriad cellular interactions in metazoans. Yet, how gap junctions control the positioning of cells in organs is not well understood. Innexins compose gap junctions in invertebrates and affect organ architecture. Here, we investigate the roles of gap-junctions in controlling distal somatic gonad architecture and its relationship to underlying germline stem cells in the nematode *Caenorhabditis elegans*. We show that a reduction of soma-germline gap-junctional signaling causes displacement of distal sheath cells (Sh1) towards the distal end of the gonad. We show that a somatically expressed innexin fusion protein, which was used as marker in a prior study asserting that the wild type lacked a bare region between the distal tip cell (DTC) and Sh1, encodes a poisonous gap junction subunit. We determine that, contrary to the model put forth in the prior study based on this marker, Sh1 mispositioning does not markedly alter the position of the borders of the stem cell pool or of the progenitor cell pool. Together, these results demonstrate that gap junctions can control the position of Sh1, but that Sh1 position is neither relevant for GLP-1/Notch signaling nor for the exit of germ cells from the stem cell pool.

Introduction

The relative positions of certain cells within larger organ structures are often important for organ function. Yet the mechanisms by which cells reach and maintain their precise relative positions within organs are poorly defined. Gap junctions act as conduits for small molecules passed between cells and/or as rivets to ensure adhesion between cells (reviewed by (Skerrett and Williams, 2017)). They have also been implicated in cell morphology within organs (reviewed by (Phelan, 2005)), however this latter role is less well characterized. Here we take advantage of well-characterized and stereotypical morphology, interactions and relationships

among cells in *Caenorhabditis elegans* to investigate the role gap junctions play in somatic gonad architecture and its consequences for the underlying germ line stem cells.

The *C. elegans* hermaphrodite gonad provides a premier system for studying organogenesis and stem cell behavior (reviewed by (Hubbard and Greenstein, 2000; Hubbard and Schedl, 2019)). Two gonad arms, anterior or posterior of a central uterus and vulva, are each capped by a single somatic cell, the distal tip cell (DTC) that establishes a stem cell niche (Figure 1). Germline stem cells and their proliferative progeny, which together are referred to as progenitors, are maintained by GLP-1/Notch mediated signaling in the germ line in response to DSL family ligands LAG-2 and APX-1 produced by the DTC (Austin and Kimble, 1987; Berry et al., 1997; Henderson et al., 1994; Nadarajan et al., 2009; Yochem and Greenwald, 1989). Proximal to the DTC, five pairs of sheath cells (named as pairs Sh1 to Sh5, distal to proximal) provide additional support (DTC and Sh1 shown in Fig. 1). In particular, Sh1 is implicated in promoting germline progenitor cell proliferation (Killian and Hubbard, 2005; McCarter et al., 1997). Although the molecular and cellular mechanisms by which Sh1 promotes germline proliferation remain to be fully elucidated, it is clear that one mechanism for the function of these cells involves the formation of gap junctions with germ cells (Starich et al., 2014).

Invertebrate gap junctions are formed from octameric hemichannels of innexin proteins (Oshima et al., 2016). In *C. elegans*, INX-8 and INX-9 associate to form hemichannels in the hermaphrodite somatic gonad which couple to germline innexin hemichannels (INX-14 with INX-21 or INX-22) to promote germline proliferation and inhibit meiotic maturation, respectively (Figure 1A-B; (Starich et al., 2014)). Phenotypic analysis of reduction-of-function mutants in *inx-8* recently led to the discovery of malonyl-CoA as a key cargo that traverses the soma-germline junction to ensure timely gametogenesis and proper embryogenesis (Starich et al., 2020) .

In the distal gonad, the somatic gonadal hemichannel components *inx-8* and *inx-9* are required redundantly for germ cell proliferation and differentiation. Loss of both components renders

the germline devoid of all but a handful of germ cells, which fail to undergo gametogenesis. Restoration of *inx-8* either to the DTC or to Sh1 rescues the severe germline proliferation defect of the *inx-8(0) inx-9(0)* double mutant, while a reduction of *inx-8* and *inx-9* via hypomorphic alleles or by RNAi limits expansion of the pool of proliferative germ cells (Dalfo et al., 2020; Starich and Greenstein, 2020; Starich et al., 2014).

Several observations point to a role for innexins in overall somatic gonad architecture. In young adult hermaphrodites, the DTC forms long extending processes reaching proximally towards Sh1, while the distal border of Sh1 is more regular, with filopodia extending distally towards the DTC. Extensive ultrastructural and both fixed and live image analysis demonstrated the existence of a "bare region" in the adult hermaphrodite gonad in which germ cells are covered only by a basal lamina in the region between the proximal extending DTC processes and the distal extending filopodia of Sh1 ((Hall et al., 1999); Figure 1). Interestingly, the hypomorphic allele *inx-14(ag17)* (Miyata et al., 2008) causes Sh1 to reach almost to the distal end of the gonad (Starich et al., 2014), obliterating the bare region between the DTC and Sh1. Similarly, a loss of the bare region was observed in *inx-8(0) inx-9(0)* double mutants in which germline proliferation was largely restored through expression of an *inx-8::gfp* transgene in the DTC only (Starich et al., 2014). This latter result suggested that if Sh1 cannot form gap junctions with germ cells, it extends distally. However, the consequences of this mis-positioning and the accompanying loss of the bare region for germline stem cells has not been previously explored.

This spatial relationship between the DTC, Sh1 and the germ line was recently challenged, and an hypothesis put forth that Sh1 might guide an oriented and asymmetric division of stem cells, such that a daughter cell in contact with Sh1 enters the differentiation pathway while the other, in contact with the DTC, remains a stem cell (Gordon et al., 2020). However, given that much of the analysis was performed using an INX-8 fusion protein marker that could conceivably alter the position of Sh1, and given that the precise relationship between the position of Sh1 vis-à-vis the border of the stem cell pool was not directly investigated, we wished to determine how

hypomorphic innexin alleles alter the position of Sh1 in live worms and whether the position of Sh1 influences the germline stem or progenitor pools.

In short, our results confirmed the presence of a bare region in the wild type and showed that reducing soma-germline gap junction coupling causes Sh1 to be mispositioned distally. Further, we determined that absence of the bare region by Sh1 distal mispositioning does not markedly alter the position of the borders of the stem or progenitor cell pools. In addition, we show that the marker used in the previous study (Gordon et al., 2020) encodes a poisonous allele of *inx-8* that also causes distal mispositioning of Sh1. Together, these results demonstrate that the position of the distal border of Sh1 is not relevant for GLP-1/Notch signaling nor for germ cells to exit the stem cell pool.

Results

Distal somatic gonad architecture is dictated by both somatic- and germline-expressed innexins

Previously, in fixed preparations, we observed that the distal edge of Sh1 was shifted almost all the way to the distal end of the gonad in worms bearing a hypomorphic mutation in the germline innexin *inx-14(ag17)* (Starich et al., 2014). We further investigated the position of the DTC relative to Sh1 in *inx-14(ag17)* using live imaging of intact young adult hermaphrodites bearing contrasting markers for Sh1 and the DTC (see Materials and Methods for details on markers used). We found that, in contrast with *inx-14(+)*, the distal edge of Sh1 in *inx-14(ag17)* extends to the distal end of the gonad, well distal to the average position of the DTC processes (Figure 1C-E). We note that this allele only moderately impairs fertility; *inx-14(ag17)* hermaphrodites display a slightly reduced average brood size of 230 progeny without appreciable embryonic lethality (Table 1).

Table 1 Brood sizes and embryonic lethality measurements for selected strains

Genotype	Brood Size[a]	Embryonic Lethality (%)
WT	292.1 ± 34.4 (n=49)	0.2 ± 0.3 (n=5843)
inx-8(qy78)[b]	108.2 ± 56.3 (n=126)	49.7 ± 17.7 (n=13,883)[c]
inx-8(qy78tn2031)[d]	270.7 ± 31.4 (n=59)	0.1 ± 0.2 (n=7748)
inx-8(tn2034)[e]	289.7 ± 43.8 (n=60)	0.1 ± 0.2 (n=7751)
inx-9(ok1502)[f]	268.8 ± 40.2 (n=72)	0.1 ± 0.2 (n=7088)
inx-8(qy102)inx-9(ok1502)[g]	144.4 ± 58.5 (n=58)	10.1 ± 8.9 (n=9303)
inx-14(ag17)[h]	230.1 ± 41.5 (n=48)	0.6 ± 0.6 (n=5192)
inx-14(ag17); inx-8(qy78) [i]	95.3 ± 33.5 (n=39)	20.3 ± 13.2 (n=4640)
bcIs39; naIs37[j]	235.8 ± 43.2 (n=56)	0.7 ± 1.2 (n=9330)

[a]Viable brood size, measured as the average number of embryos that hatch from single parent at 20ºC.

[b]DG5063 (n=95) and DG5261 (n=31). DG5063 was derived from the strain NK2571 *inx-8(qy78); cpIs122(lag-2p::mNeonGreen::plcdeltaPH)* (Gordon et al., 2020) by outcrossing with wild-type males. DG5261 was generated from DG5063 by outcrossing with wild-type males. We examined NK2571 and observed an average brood size of 155 ± 24.4 (n=19) with 58.2 ± 14.9% embryonic lethality (n=4056).

[c]The percentage of embryonic lethality (Emb) is increased early and late in the brood, with the following breakdown: Day 1, 87.7% Emb (n=922); Day 2, 65.0% Emb (n=4743); Day 3, 29.6% Emb (n=6047); Day 4, 32.2% Emb (n=1835); Day 5, 61.1% Emb (n=337).

[d]DG5250 was derived from *inx-8(qy78)* by deleting the mKate2 moiety and additional *inx-8* sequences to generate an *inx-8* null allele.

[e]DG5251. This strain has the same DNA sequence at the *inx-8* locus as does the *inx-8(qy78tn2031)* null allele, but it was generated in an otherwise *inx-8(+)* background, not in *qy78*.

[f]DG5059, an *inx-9* null allele.

[g]DG5064. *inx-8(qy102)* is the mKate2:INX-8 fusion generated in the *inx-9(ok1502)* genetic background (Gordon et al., 2020). DG5064 was derived from NK2576 *inx-9(ok1502) inx-8(qy102[mKate2::inx-8]); cpIs122(lag-2p::mNeonGreen::plcdeltaPH)* by out-crossing with wild-type males. We examined NK2576 and observed an average brood size of 168.6 ± 83.9 (n=20) with 11.2 ± 6.3% embryonic lethality (n=3595).

[h]DG5270. INX-14R326H (Miyata et al., 2008; Starich et al., 2014).

[i]DG5070

[j]DG5020 Strain with sheath and DTC markers but otherwise wild-type.

To determine whether the position of Sh1 is also shifted distally upon reduction of the somatic innexins, we investigated the position of Sh1 relative to the distal end of the gonad in a well-characterized compound *inx-8* mutant ((Starich et al., 2020); Figure 1B-E). We found that Sh1 in worms bearing one partially functional somatic gonad innexin encoded by *inx-8(tn1513tn1555)* in an otherwise null *inx-9(ok1502)* background (hereafter referred to as "*inx-8(rf)*"; (Starich et al., 2020)), is also distally positioned, similar to *inx-14(ag17)* (Figure 1C-E). The existence of the bare region in wild-type worms, as well as the distally altered Sh1 position in the *inx-14* and *inx-8* mutants were consistent in live images of worms bearing different DTC and sheath markers (Figure 1—figure supplement 1).

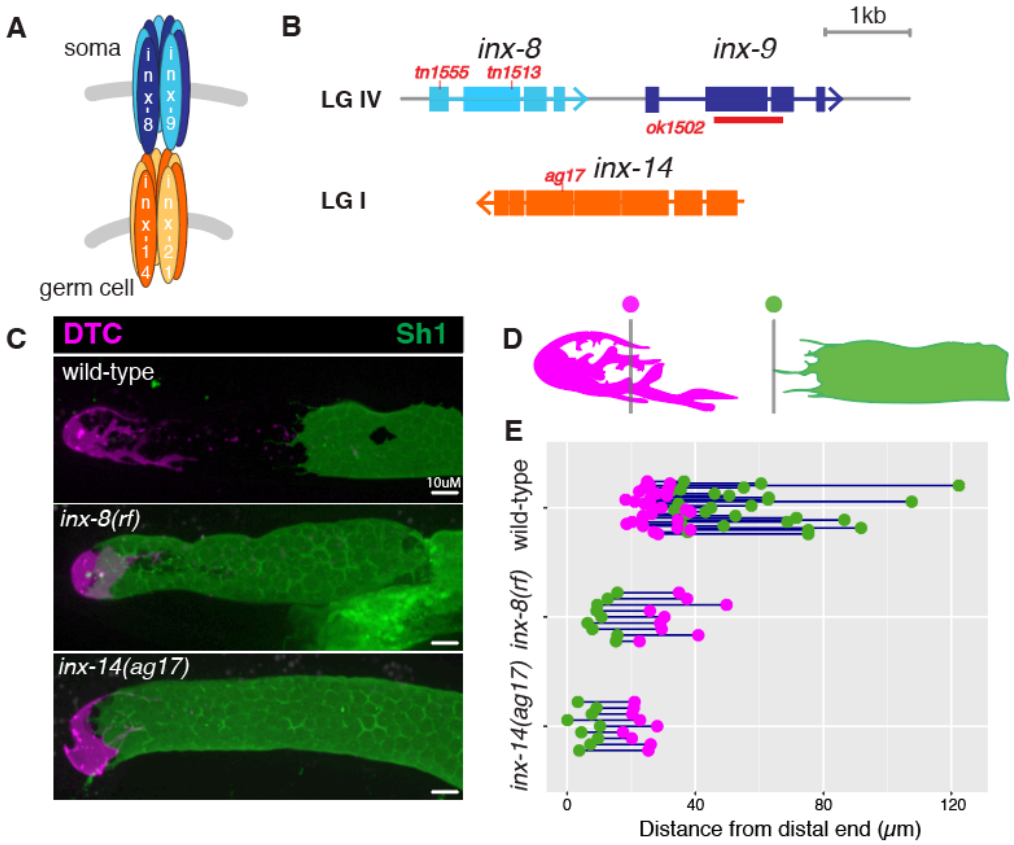

Figure 1. Germline and somatic gonad innexins are required for proper somatic gonad architecture. A. Schematic of paired somatic and germline octameric hemichannels. B. Schematic diagram of the *inx-8 inx-9* locus and the *inx-14* locus, with relevant mutations indicated in red. C. Fluorescent confocal maximum projection images of distal gonads in live worms. Distal tip cell (DTC) marked in magenta (*naIs37[lag-2p::mCherry-PH]*) and sheath pair 1 (Sh1) marked in green (*bcIs39[lim-7p::CED-1::GFP]*). Top: strain bearing markers only, denoted "wild type". Middle: *inx-8(tn1513tn1555) inx-9(ok1502)*, denoted "*inx-8(rf)*" after Starich et al. (2020). Bottom: *inx-14(ag17)*. D. Diagram of DTC-Sh1 relationship in distal end of a typical wild-type gonad (DTC magenta, Sh1 green). Although these cells have variable morphology, certain parameters can be measured for each specimen, as indicated in Figure 1– figure supplement 1. A vertical line topped with a magenta dot shows the average length of contiguous DTC processes for that gonad and a vertical line with a green dot shows the most distal extent of the sheath cell. A detailed diagram of all measurements taken for live fluorescent images is shown in Figure 1–figure supplement 1. E. Plot showing the distance between the average DTC process length (magenta dots) and the most distal extent of the sheath cell (green dots); each pair of dots joined by a blue line represents the data for a single gonad. The presence of a bare region is indicated when the green dot is to the right of the magenta dot; absence of a bare region is indicated when the green dot is to the left of the magenta dot.

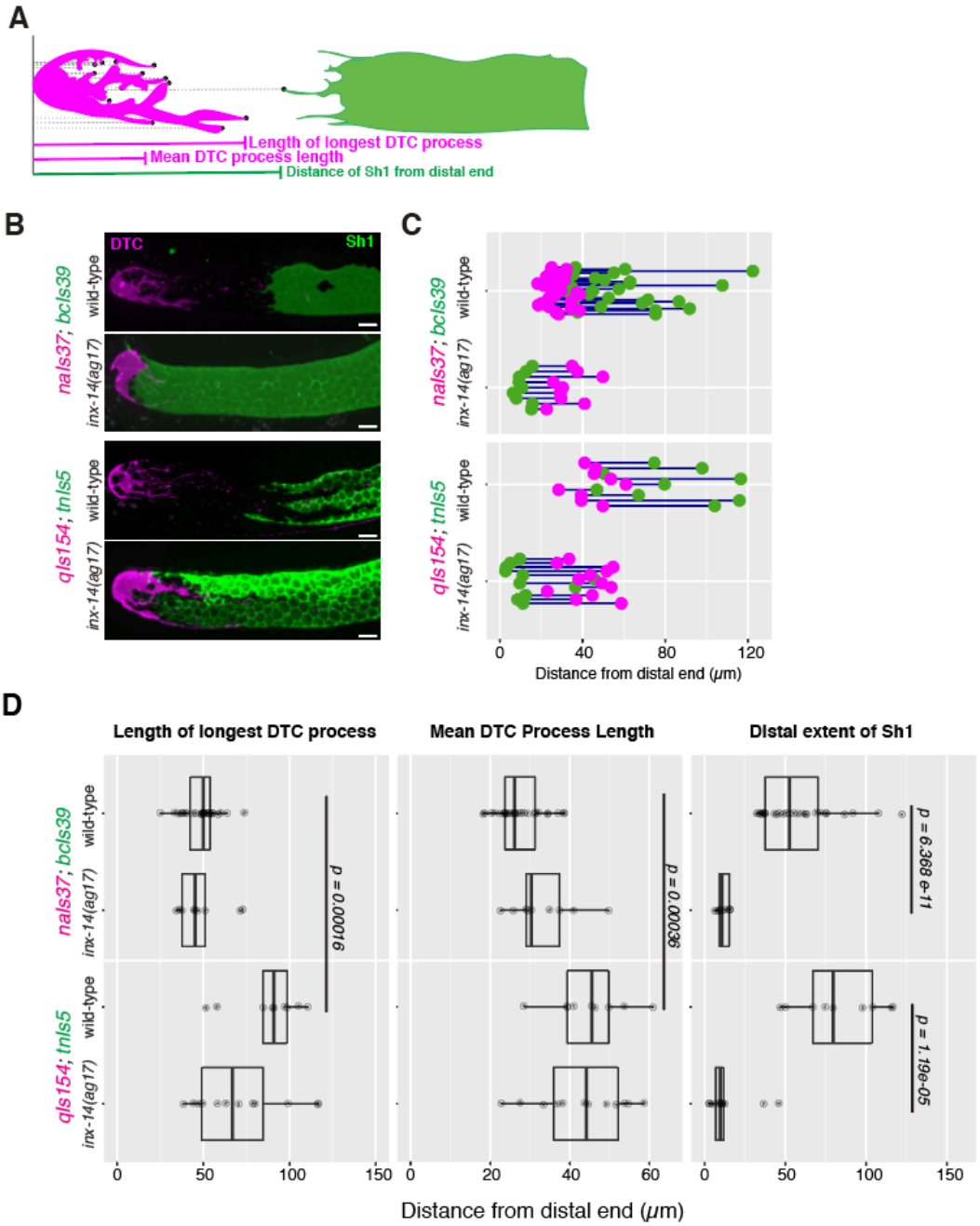

Figure 1—figure supplement 1. Consistent trends in Sh1 and DTC positions are observed with multiple markers. A. Schematic diagram of DTC and sheath parameters measured in this study. Each black dot represents a point in a maximum projection Z-stack for which the distance from the distal end was measured in microns. B. Fluorescent micrographs of gonads in live worms bearing *naIs37[lag-2p::mCherry-PH]* and *bcIs39[lim-7p::CED-1::GFP]* (top pair, same images as in Fig. 1, included here for comparison) or *qIs154[lag-2p::myr-tdTomato]* and *tnIs5[lim-7p::GFP]*

(bottom pair), in wild-type and *inx-14(ag17)* mutant backgrounds, as indicated. C. Quantitative plot with magenta dots representing the average length of DTC process paired to green dots representing the distal extent of Sh1. Each pair of dots connected by a line represents data for a single gonad. The presence of a bare region is indicated when the green dot is to the right of the magenta dot; absence of a bare region is indicated when the green dot is to the left of the red dot. D. Plots showing quantitative measurement of parameters diagrammed in (A). Although the behavior of the DTCs marked by different markers is variable, and DTCs marked with *qIs154* show significantly longer DTC processes, the behavior of Sh1 in the presence of either marker shows significantly consistent changes across mutant genotypes. All p-values result from Student's t-test. Scale bar is 10µm.

An mKate2::INX-8 fusion encodes a poisonous INX-8 protein

We extended our analysis to *inx-8(qy78[mKate2::INX-8])*, an allele that encodes a fusion protein of mKate2 and INX-8 that was used to mark Sh1 in a prior study (Gordon et al., 2020). We found that, like *inx-14(ag17)* and *inx-8(rf)*, *inx-8(qy78)* caused a distal shift in Sh1 (Figure 2). In addition, this allele causes a severe reduction in brood size and highly penetrant embryonic lethality (Table 1). We also observed that this same deletion in the background of the *inx-9* null mutant (*inx-8(qy102)*, see Materials and Methods) shifts Sh1 even more distally, whereas loss of *inx-9* alone does not significantly affect Sh1 position (Figure 2—figure supplement 1).

To ensure that the apparent distal shift of Sh1 in the *inx-8(qy78[mKate2::INX-8])* background did not reflect a disparity between the expression patterns of mKate2::INX-8 and either of the *lim-7p*-driven Sh1 markers, we examined the overlap between the mKate2::INX-8 and *lim-7p*-driven markers in strains expressing both *inx-8(qy78[mKate2::INX-8])* and GFP markers encoded by *tnIs6* [*lim-7p::GFP*] or *bcIs39* [*lim-7p::CED-1::GFP*] (Figure 2—figure supplement 2). In short, in over 85% of gonad arms examined, the overlap was complete. In short, in over 85% of gonad arms examined, the overlap was complete. In both cases, the remaining gonads displayed reduced Sh1 expression, which may be the result of stochastic transgene downregulation.

Based on our observations that *inx-8(qy78*[mKate2::INX-8]*)* displays embryonic lethality and a distal shift in the border of Sh1, we hypothesized that *inx-8(qy78)* might encode a poisonous

INX-8 protein. If so, we would predict that the distal shift of Sh1, the reduced brood size, and embryonic lethality seen with this allele would be dependent on the presence of the INX-8 coding region. To test this hypothesis, we used CRISPR-Cas9 genome editing to generate *inx-8* null alleles in both the *inx-8(qy78[mKate2::inx-8])* and wild-type genetic backgrounds. We generated deletions with identical breakpoints in the *inx-8* locus in both genetic backgrounds [e.g., *inx-8(qy78tn2031)* and *inx-8(tn2034)*] starting 136 bp upstream of the wild-type *inx-8* ATG start codon and extending 221 bp into *inx-8* exon 3 (Figure 2 and Figure 2—figure supplement 1). In the *inx-8(qy78[mKate2::inx-8])* context, this deletion also removes the mKate2 moiety. These deletions are expected to constitute *inx-8* null alleles because, in addition to removing the start codon, they delete amino acids 1–349 (out of 382 amino acids), including virtually all residues essential for spanning the plasma membrane and forming a channel (Starich and Greenstein, 2020). These deletions must not appreciably perturb the function of *inx-9* because they exhibit nearly normal brood sizes (Table 1). Unlike the original *inx-8(qy78)* allele, the compound mutant *inx-8(qy78tn2031)* almost completely restores the DTC-Sh1 positional relationship with a substantial return of the bare region (Figure 2). Further, *inx-8(qy78 tn2031)* exhibits a nearly normal brood size and suppresses the embryonic lethality observed in the *inx-8(qy78)* starting strain (Table 1). Likewise, the identical deletion generated in the wild-type genetic background [e.g., *inx-8(tn2034)*] also exhibits a substantial bare region (Figure 2—figure supplement 1) with a normal brood size and negligible embryonic lethality (Table 1). Thus, we conclude that *inx-8(qy78)* encodes a poisonous mKate2::INX-8 product that interferes with the normal channel and/or rivet functions of soma-germline gap junctions.

A surprising observation was that both the *inx-14(ag17)* mutation and the *inx-9(ok1502*) null mutation could individually suppress the embryonic lethality caused by an mKate2::INX-8 fusion protein (Table 1). Because it has been shown that gap junctions in the proximal gonad are required for embryonic development by virtue of their function to deliver malonyl-CoA to developing oocytes (Starich et al., 2020), one possibility is that mKate2::INX-8-containing channels are constitutively or too-widely open such that embryos receive inappropriately large amounts of transiting biomolecules, and that this can be compensated by reducing channel

function. Alternatively, possible delays in gametogenesis that may occur in the double mutants might effectively increase oocyte quality by providing additional time for levels of needed biomolecules to build up in the germ line. Perhaps favoring this second possibility is an unusual behavior of *inx-8(qy78)* itself: the first embryos produced in the brood display heightened embryonic lethality, suggesting that if key limiting substances fail to accumulate early, a time-dependent or later mechanism may compensate.

In any case, the genetic behavior of *inx-8(qy78)* suggests that this mutant allele confers both loss-of-function and antimorphic properties to soma-germline gap junctions. We infer loss-of-function behavior since other loss-of-function mutations affecting soma-germline gap junctions, such as *inx-14(ag17),* also cause a loss of the bare region, though *inx-14(ag17)* does so without reducing brood size or embryonic viability (Table 1). We infer antimorphic behavior of *inx-8(qy78)* since removing the entire protein suppresses all defects, including loss of the bare region, brood size and embryonic viability.

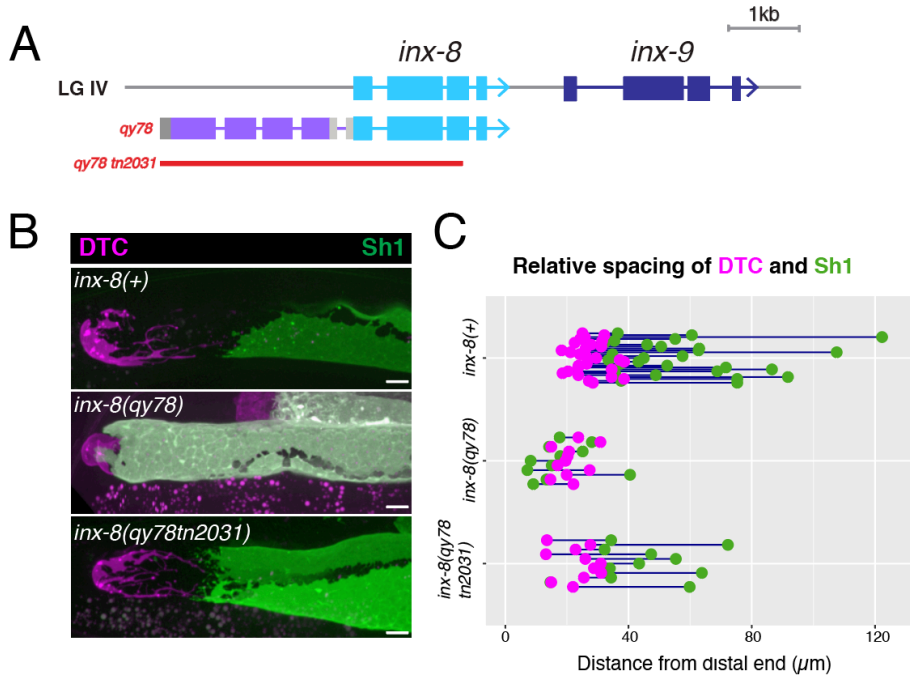

Figure 2. N-terminal fusion of mKate2 to INX-8 generates a poisonous INX-8 protein that alters somatic gonad morphology. A. Schematic diagram showing the genetic manipulations used in this section. *inx-8(qy78)* was created by placing mKate2 in-frame with the N-terminus of INX-8 (Gordon et al., 2020). *inx-8(qy78tn2031)* was created by deleting the *inx-8* coding region and mKate2 moiety in the *inx-8(qy78)* background. B. Fluorescent micrographs of live animals with the DTC marked by *naIs37[lag-2p::mCherry-PH]* and Sh1 marked by *bcIs39[lim-7p::CED-1::GFP]*. Top: wild-type with markers only. Middle: *inx-8(qy78)*. Bottom: *inx-8(qy78tn2031).* C. Quantitative dot-plot with magenta dots showing average length of DTC processes and green dots showing distal extent of Sh1. Data for wild-type (marker only) strain in C is the same as in Figure 1. Each pair of dots connected by a line represents data for a single gonad. Scale bar 10µm.

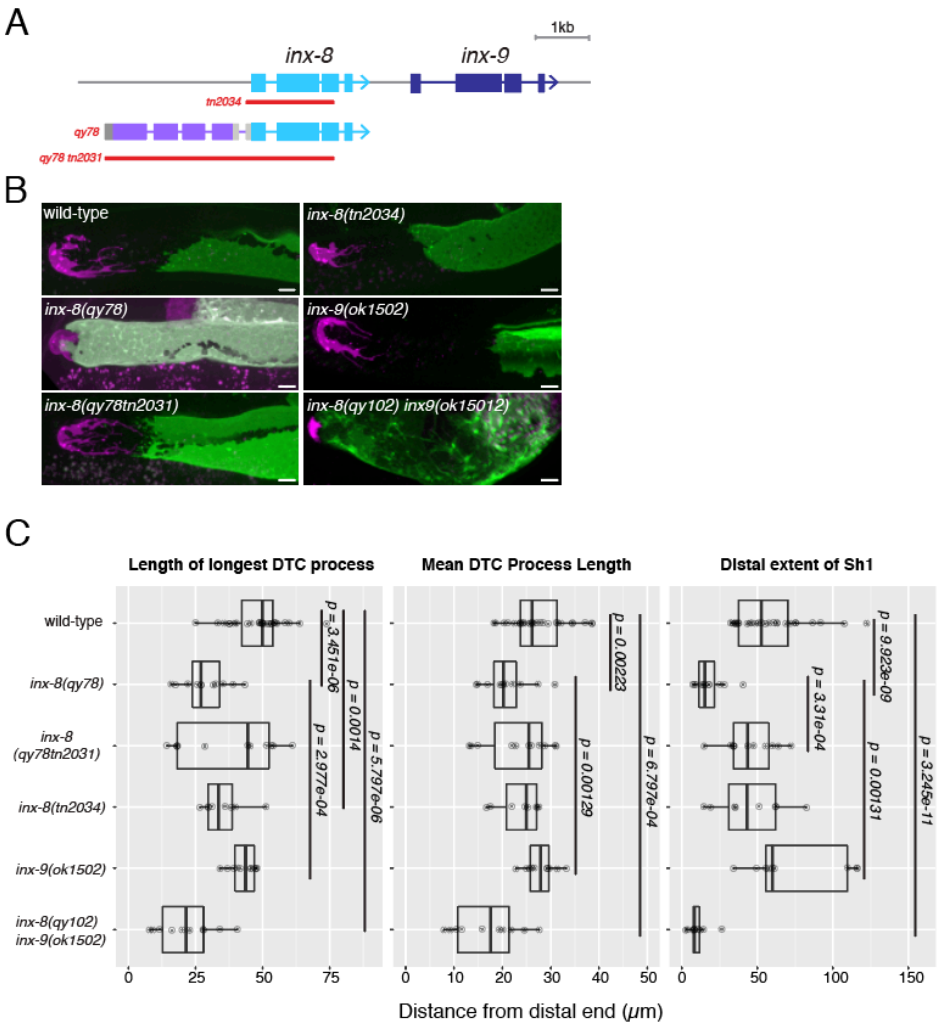

Figure 2–figure supplement 1. Additional evidence that the *qy78 mKate2::inx-8* fusion generates a poisonous INX-8 protein. A. Schematic diagram showing additional alleles at the *inx-8 inx-9* loci that affect somatic gonad architecture. B. Representative fluorescent micrographs of live worms carrying each relevant allele (images for *inx-8(+), inx-8(qy78)* and *inx-8(qy102tn2031)* are the same as in Fig. 2B, included here for comparison). C. Quantitative plots showing changes to DTC morphology and Sh1 position. All p-values result from Student's t-test. Scale bar 10µm.

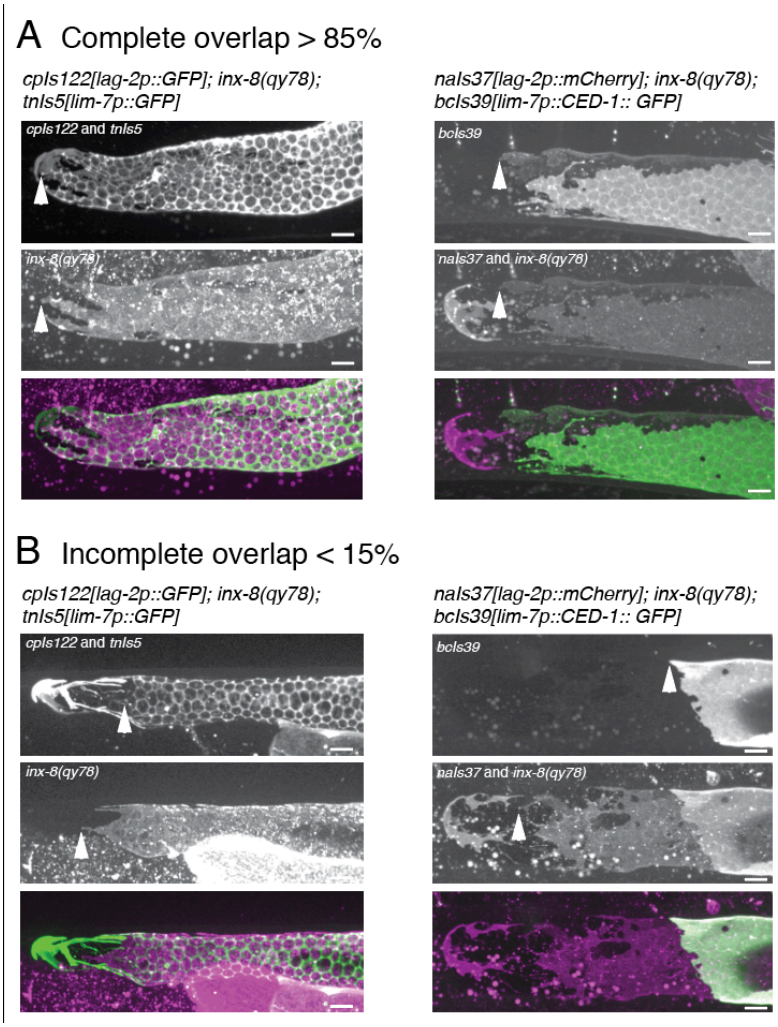

Figure 2—figure supplement 2. The low-penetrance loss of marker expression in Sh1 does not reflect altered sheath cell placement. A. Individual gonads carrying different Sh1 markers in addition to *inx-8(qy78[mKate2::INX-8])* Left column: Individual channels and merged image (bottom panel) of a single worm co-expressing the DTC marker *cpIs122[lag-2p::GFP], inx-8(qy78[mKate2::INX-8])* and the sheath cell marker *tnIs5[lim-7p::GFP]*. Of 33 gonads examined, 30 showed perfect overlap as shown in these images. Right column: Individual channels and merged image (bottom panel) of a single worm co-expressing the DTC marker *naIs37[lag-2p::mCherry-PH], inx-*

8(qy78[mKate2::INX-8]) and the sheath cell marker *bcIs39[lim-7p::CED-1::GFP]*. Of 13 gonads examined, eleven showed complete overlap. B. Two individual gonads of the same genotypes as in (A), showing incomplete overlap between mKate2::INX-8 and the respective GFP sheath cell markers. White arrowheads mark the most distal extent of each marker in the single-channel panels. Scale bars are 10μm.

The distal position of Sh1 does not influence the position of the stem cell pool border

A recent model proposed that the position of the Sh1 border influences the stem/non-stem decision in underlying germ cells (Gordon et al., 2020). However, because the previous study did not examine the position of stem or progenitor cells, and because the model was based on results using the poisonous *inx-8(qy78)* allele, we investigated this relationship.

In its simplest form, the model predicts that when the distal edge of Sh1 is positioned distally, the stem/non-stem border should similarly shift distally. The SYGL-1 protein serves as a stem cell marker as *sygl-1* is a direct transcriptional target of GLP-1/Notch in the germ line (Brenner and Schedl, 2016; Chen et al., 2020; Kershner et al., 2014; Lee et al., 2019; Lee et al., 2016; Shin et al., 2017). We analyzed the proximal extent of the pool of SYGL-1-positive cells bearing a well-characterized OLLAS epitope tag on SYGL-1 and compared that boundary relative to the distal Sh1 border (Figure 3 and Materials and Methods). In the case of *inx-14(ag17),* though the distal border of Sh1 was shifted drastically and significantly, there was no significant change in the size of the SYGL-1-positive stem cell pool. In the case of the *inx-8(qy78[mKate2::inx-8])* allele, the border of the SYGL-1-positive pool was marginally shifted distally relative to the wild type, though not commensurate with the extent to which Sh1 shifted distally in this background. Furthermore, the shifted border of the stem cell pool was suppressed when *inx-8* was deleted, either in *inx-8(qy78tn2031)* on in *inx-8(tn2034),* suggesting that such a defect was due to the altered function of mKate2::INX-8, rather than due to the position of Sh1 (Figure 3A-C). To detect any subtle correlation between the proximal end of the SYGL-1 pool and the distal extent of Sh1, we plotted these against each other and computed an R value (Figure 3D). By

Pearson correlation, there is no significant relationship in any genotype examined between the position of the sheath cell, and the extent of the SYGL-1(+) stem cell pool.

The recent model also proposed that Sh1 controls spindle orientation at the stem/progenitor border. However, we found that in the wild type (marker-only) strain, the distal position of Sh1 was proximal to the proximal SYGL-1-positive border in 86% of the gonads (276/320), with the distance 5 cell diameters or greater in 67% of gonads (215/320) (Figure 3 and Figure 3—figure supplement 1). This 5 cell-diameter distance is not consistent with the hypothesis that Sh1 is controlling spindle orientation at the border as such control would be expected to occur over a distance of 1-2 cell diameters.

We conclude that there is no correlation between the position of the distal border of Sh1 and the proximal border of the SYGL-1-positive stem cell pool and that if spindle-oriented divisions occur at the Sh1 border, they are not influencing cell fate.

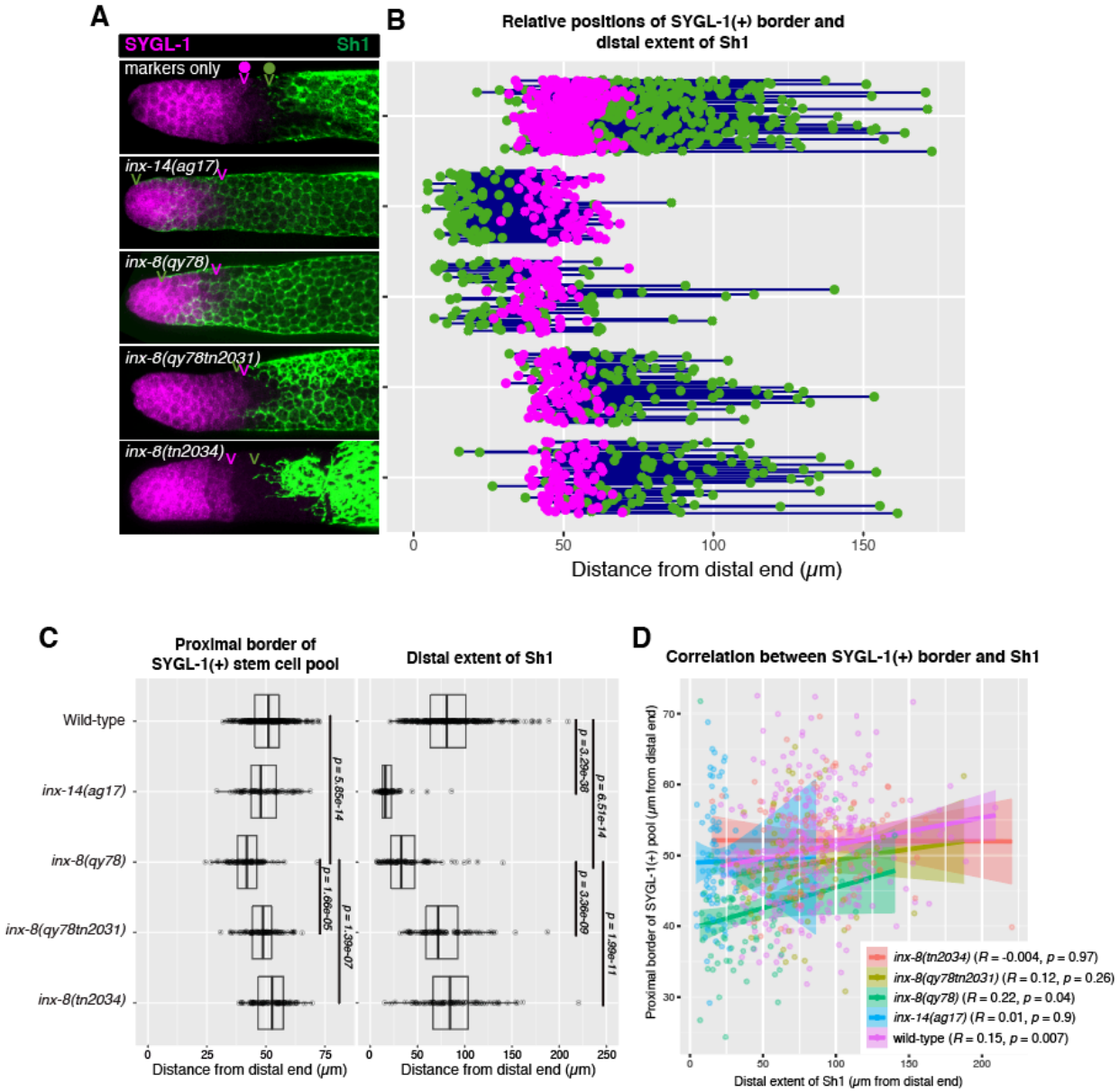

Figure 3. The position of the proximal border of the SYGL-1-positive stem cell pool does not correlate with the position of Sh1. A. Fluorescent confocal maximum projection images of fixed, dissected gonads showing the SYGL-1(+) stem cell pool marked in magenta and the sheath cell marked in green. Magenta caret represents the location of the proximal border of the SYGL-1(+) stem cell pool. Green caret represents the distal edge of Sh1. B. Quantitative graph with magenta dots representing the proximal border of SYGL-1::OLLAS expression and green dots representing the distal reach of Sh1. Each pair of dots connected by a line represents the data for a single

gonad. C. Dot plot with overlaid box plots showing the size and quantiles of the SYGL-1(+) stem cell pool and distal extent of Sh1 for each genotype. Each dot represents a single specimen of that genotype. P-values were calculated using Student's t-test. D. Scatterplot showing lack of correlation between the proximal extent of SYGL-1 expression and the distal reach of Sh1.

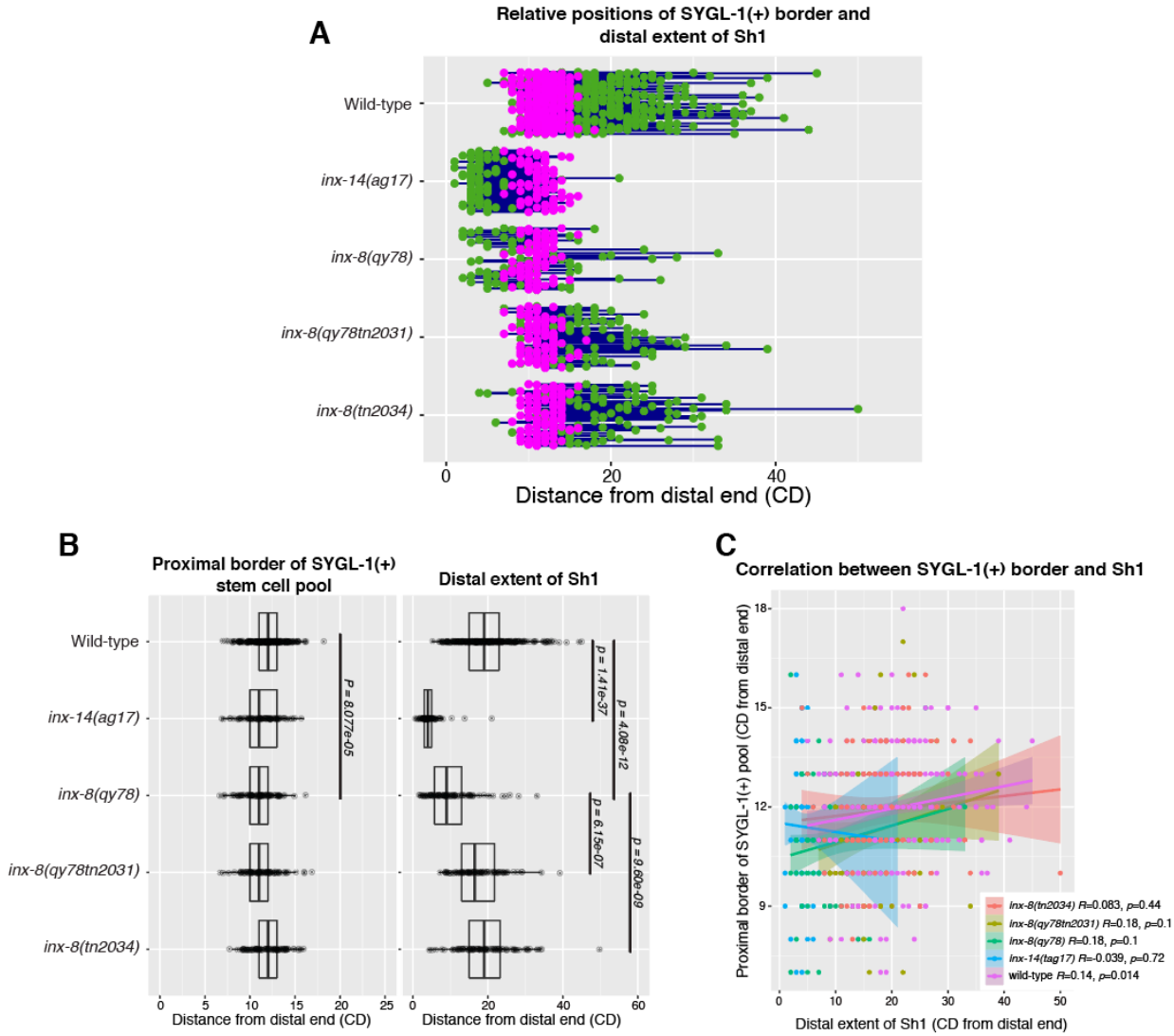

Figure 3—figure supplement 1. The position of the proximal border of the SYGL-1-positive stem cell pool does not correlate with the position of Sh1 when data are shown in cell diameters. A. Quantitative graph with magenta dots representing the proximal extent of SYGL-1::OLLAS expression and green dots representing the distal reach of Sh1. Each pair of magenta and green dots connected by a line represents the data for a single gonad. B. Dot plot with

overlaid box plots showing the size and quantiles of the SYGL-1(+) stem cell pool and distal extent of Sh1 for each genotype, in cell diameters from the distal end. Each dot represents a single specimen of that genotype. P-values were calculated using Student's t-test. C. Scatterplot showing lack of correlation between the proximal extent of SYGL-1 expression and the distal reach of Sh1. CD: cell diameters.

The Distal position of Sh1 does not influence the position of the progenitor pool border

Although we found no correlation between the stem cell pool border and Sh1 position, we wondered whether altered Sh1 position might nevertheless influence the position of the border between the progenitor zone (PZ) and the transition zone that marks overt meiotic entry. In wild type, we found that the distal position of Sh1 can be either distal or proximal of the PZ border, using the length of the CYE-1-positive region to define the PZ border, following CYE-1 and pSUN-1(S8) co-staining (Figure 4 and Materials and Methods; Mohammad et al., 2018). We found that although there is a subtle shift in the PZ border in *inx-8(qy78)* and *inx-14(ag17)*, it does not correlate with the dramatic shift in Sh1 position seen in these mutants (Figure 4).

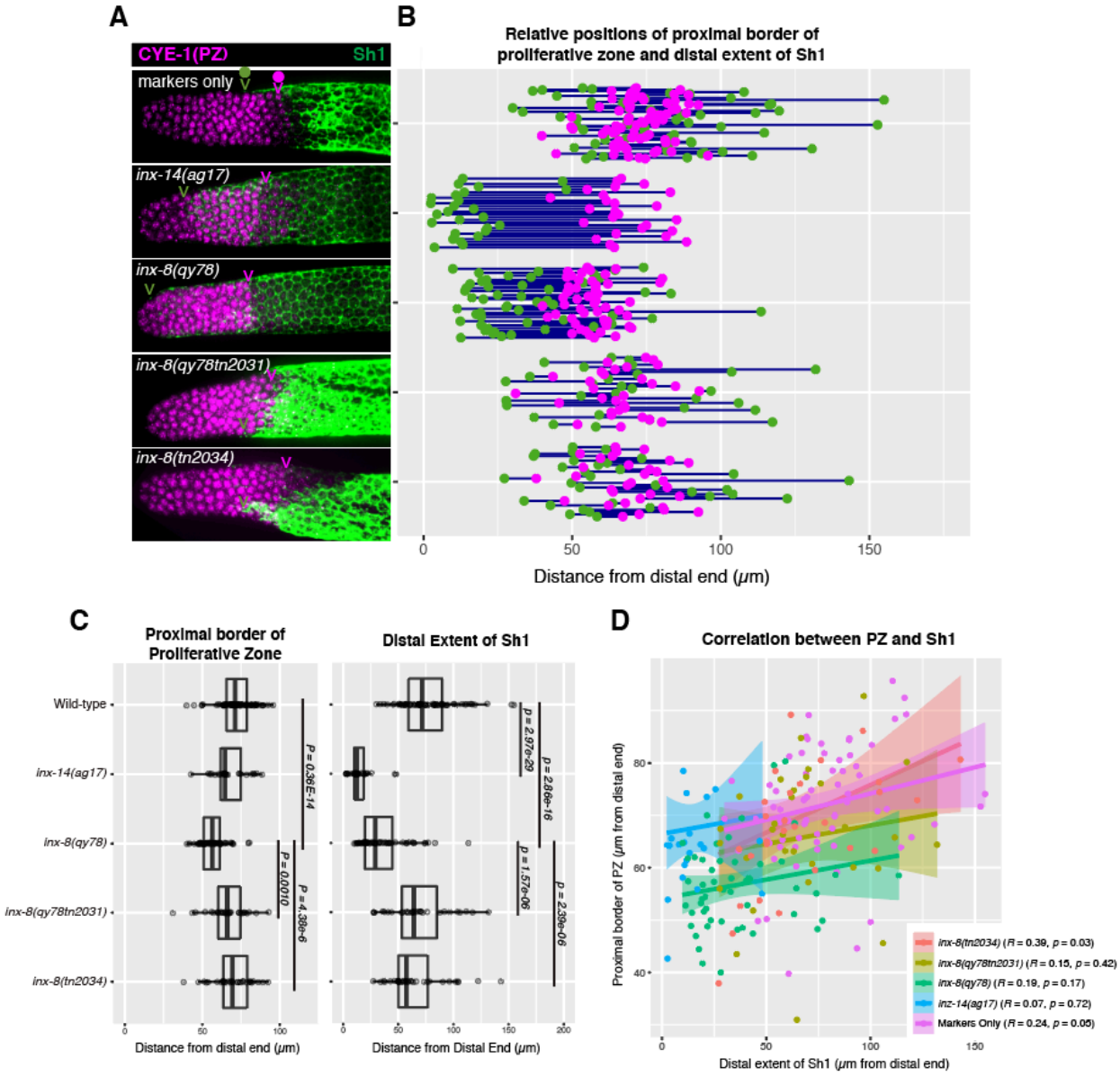

Figure 4. The position of the proximal border of the progenitor zone does not correlate with the position of Sh1. A. Fluorescent confocal maximum projection images of fixed, dissected gonads showing the progenitor pool marked in magenta and the sheath cell marked in green. Magenta caret represents the location of the proximal border of the CYE-1(+),pSUN-1(-) progenitor pool. Green caret represents the distal edge of Sh1. B. Quantitative graph with magenta dots representing the proximal extent of the CYE-1 staining and green dots representing the distal reach of Sh1. Each pair of magenta and green dots connected by a line represents the data for a single gonad. C. Dot plot with overlaid box plots showing the size and quantiles of the progenitor pool and distal extent of Sh1 for each genotype. Each dot represents a single specimen of that genotype. P-values were calculated using Student's t-test. D. Scatterplot showing that lack of correlation between the proximal PZ border and Sh1 position.

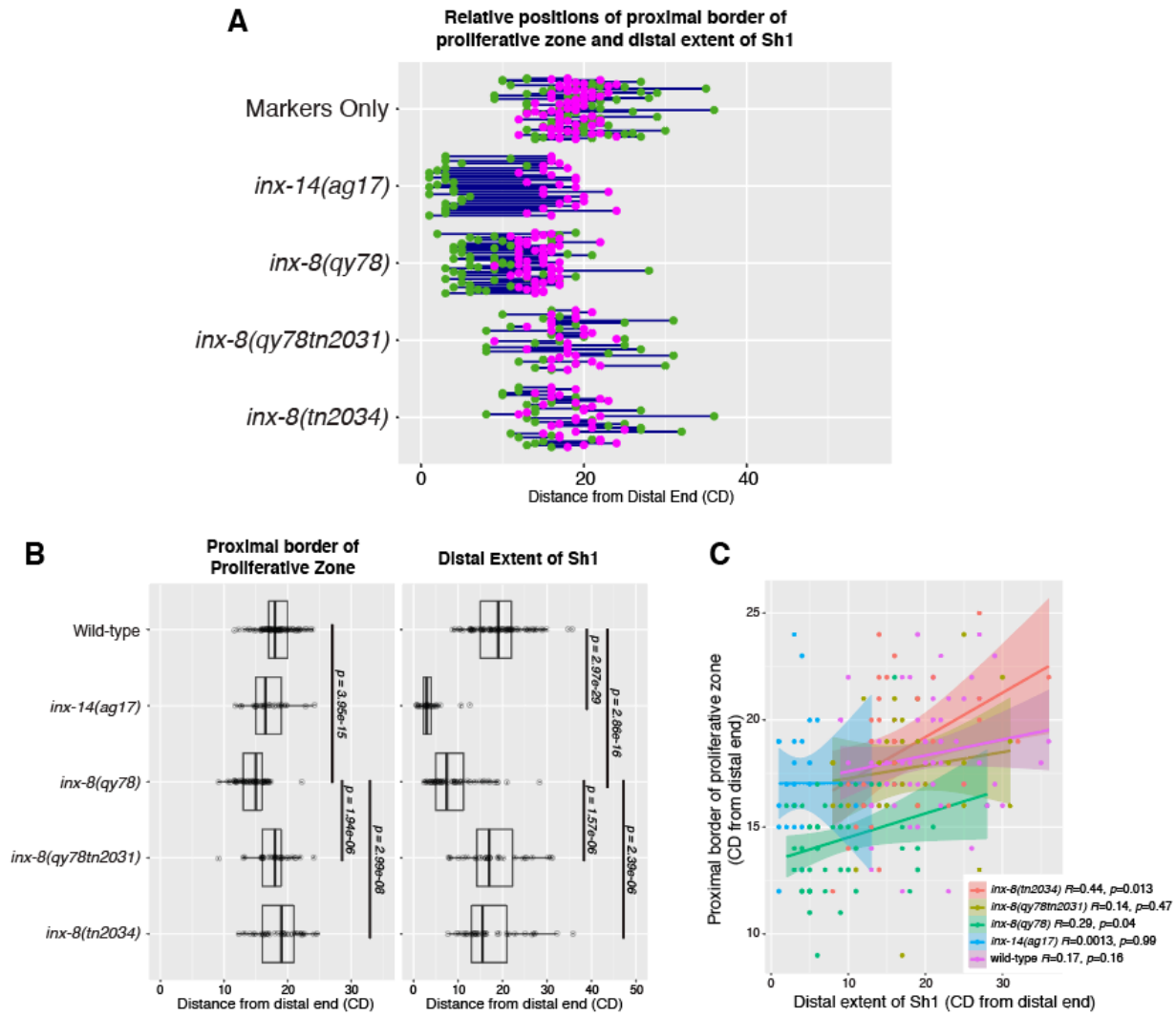

Figure 4–figure supplement 1. The extent of the proliferative zone does not correlate with the position of Sh1 when data are shown in cell diameters. A. Quantitative graph with magenta dots representing the location of the proximal border of the CYE-1(+), pSUN-1(-) progenitor pool and green dots representing the proximal extent of and green dots representing the distal reach of Sh1. Each pair of magenta and green dots connected by a line represents the data for a single gonad. B. Dot plot with overlaid box plots showing the size and quantiles of the CYE-1(+) progenitor pool and distal extent of Sh1 for each genotype, in cell diameters from the distal end. Each dot represents a single specimen of that genotype. P-values were calculated using Student's t-test. C. Scatterplot showing lack of correlation between the proximal extent of proliferative zone and the distal reach of Sh1. CD: cell diameters.

412

413

414 **Discussion**

415

416 These studies show that impaired innexin function distally displaces sheath cells, but that this
417 displacement does not similarly shift the proximal border of the stem cell pool (Figure 5). We
418 show that a gap normally exists between the DTC and Sh1, but that this gap can be closed with
419 reduced innexin activity either in the soma or the germ line. These results contradict a previous
420 observation that relied on a marker that was itself interfering with innexin function. The
421 cautionary tale is that fusion proteins used as markers, even when they are generated by
422 CRISPR/Cas9 genome editing in the context of the endogenous locus and therefore are not
423 likely mis-expressed or overexpressed, may nevertheless generate poisonous proteins. Here,
424 the mKate2::INX-8 fusion protein caused a distal shift in the Sh1 position due to its apparent
425 antimorphic effect on gap junctions. Because of the redundant function of INX-9, we were able
426 to remove the offending mKate2::INX-8 protein entirely and restore the bare region. Our
427 finding that the germline response to signaling from the DTC, as measured by expression of the
428 GLP-1/Notch target, SYGL-1, is independent of interactions with distal sheath cells also meshes
429 with the finding that males, which lack distal sheath cells altogether, exhibit similarly sized stem
430 cell pools (Crittenden et al., 2019). In addition, the distal border of Sh1 relative to the proximal
431 stem cell border in the wild type is ≥5 cell diameters in the majority of gonads examined. Thus,
432 the previous model that Sh1 acts to orient divisions of stem cells to thereby direct their fate is
433 also called into question by our results. Finally, using alleles that dramatically alter the position
434 of Sh1, we found no evidence supporting the prediction that the stem/non-stem border is
435 coincident with the Sh1 border. Together, these results indicate that Sh1 is not involved in the
436 germline stem-progenitor fate decision.

437

438 Our studies also provide evidence that innexin gap junctions not only serve as communication
439 and adhesion junctions, but that in the context of an organ system they contribute to the
440 positioning of cells relative to each other. How might gap junctions influence the relative

position of the DTC and Sh1 in the distal gonad arm? The DTC also forms gap junctions with germ cells, which must be disassembled as germ cells enter the bare region, only to be reassembled again when in contact with Sh1 (and then again with the more proximal sheath cells). A detailed TEM analysis of the gonad (Hall et al., 1999) led to the consideration that a constant interplay of association and dissociation likely also occurs between Sh1 and the underlying germ cells that migrate proximally along the arm: as germ cell flux continually moves germ cells towards the proximal end of the gonad, the Sh1 cells presumably extend their filopodia distally and form new gap junction connections with incoming germ cells. Otherwise, the bare region would increase in size. The relative steady-state positions of the DTC and Sh1 may therefore be determined by the rate of germ cell proliferation as well as by the strength of interaction between Sh1 and germ cells, and gap junctions could contribute to both.

To complement the role of gap junctions in promoting robust proliferation, the kinetics of gap junction coupling between the somatic gonad and germ cells may play a role in determining the strength of the interactions between the two cell types. Unlike sheath-oocyte junctions, which form large plaques containing many functional gap junctions, the gap junctions formed in the distal arm appear to represent looser associations of a few gap-junction channels (Starich et al., 2014). Nonetheless, these associations may be sufficient to maintain adhesion with the underlying germline, functioning like regularly spaced rivets, albeit dynamic and removeable ones.

Disentangling the adhesive and channel functions of gap junctions is a complex issue. The mutants used in this study are competent to form gap junctions. However, they may do so less efficiently than their wild-type counterparts. For example, the pattern of localization of gap junction puncta in *inx-8(rf)* and *inx-14(ag17)* appears more diffuse than in the wild type (Starich et al., 2014);(Starich et al., 2020). Alternatively or additionally, the mutants in this study may assemble into hemichannels as readily as the wild-type, but the pairing or opening of gap junction channels may be compromised. Studies of connexin gap-junction channels in paired Xenopus oocytes strongly suggest that opening of hemichannels facilitates their assembly into

gap junctions. That study proposed hemichannel opening collapses the intermembrane space between juxtaposed cells to allow the extracellular loops of connexins to dock into gap junctions (Beahm and Hall, 2004). If a similar model applies to innexin-containing gap junctions, then rivet and channel function would be coupled.

How could impaired innexin function cause Sh1 to creep more distally? One hypothesis is that when fewer junctions are made, reduced adhesion or reduced recognition occurs. This scenario would also be consistent with Sh1 extending to the distal end when no gap junctions can form between sheath cells and germ cells (Starich et al., 2014). At the same time, it is not possible to exclude the formal possibility that the DTC and Sh1 engage in an active repellent or passive space-excluding interaction that somehow involves gap junction function. Another possibility is that a deficit in gap-junctions might be sensed by Sh1, which then responds by extending its coverage of the germ line to increase the surface area over which junctions may form to supply more of the active biomolecules that transit through these junctions. Nevertheless, our studies show that the position of germline stem cells is independent of the position of Sh1.

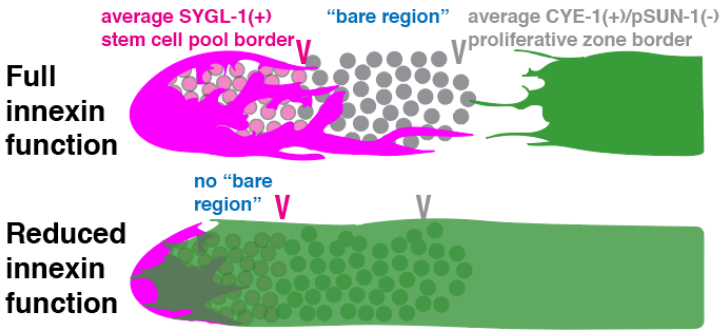

Figure 5. Reduced innexin function eliminates the bare region between the DTC and Sh1, but this shift does not alter the border of the stem cell pool.

Acknowledgements

We thank Gabriela Huelgas-Morales for discussions and constructive suggestions during the course of this work, and we thank Swathi Arur for the affinity purified anti-GFP antibody. We thank WormBase. The CGC, which is funded by NIH Office of Research Infrastructure Programs (P40 OD010440), provided some starting strains.

References

Arribere, J.A., Bell, R.T., Fu, B.X., Artiles, K.L., Hartman, P.S., Fire, A.Z., 2014. Efficient marker-free recovery of custom genetic modifications with CRISPR/Cas9 in Caenorhabditis elegans. Genetics 198, 837-846.

Austin, J., Kimble, J., 1987. glp-1 is required in the germ line for regulation of the decision between mitosis and meiosis in C. elegans. Cell 51, 589-599.

Beahm, D.L., Hall, J.E., 2004. Opening hemichannels in nonjunctional membrane stimulates gap junction formation. Biophys J 86, 781-796.

Berry, L.W., Westlund, B., Schedl, T., 1997. Germ-line tumor formation caused by activation of glp-1, a Caenorhabditis elegans member of the Notch family of receptors. Development (Cambridge, England) 124, 925-936.

Brenner, J.L., Schedl, T., 2016. Germline Stem Cell Differentiation Entails Regional Control of Cell Fate Regulator GLD-1 in Caenorhabditis elegans. Genetics 202, 1085-1103.

Brodigan, T.M., Liu, J., Park, M., Kipreos, E.T., Krause, M., 2003. Cyclin E expression during development in Caenorhabditis elegans. Dev Biol 254, 102-115.

521 Byrd, D.T., Knobel, K., Affeldt, K., Crittenden, S.L., Kimble, J., 2014. A DTC niche plexus
522 surrounds the germline stem cell pool in Caenorhabditis elegans. PLoS One 9, e88372.
523
524 Chen, J., Mohammad, A., Pazdernik, N., Huang, H., Bowman, B., Tycksen, E., Schedl, T., 2020.
525 GLP-1 Notch-LAG-1 CSL control of the germline stem cell fate is mediated by transcriptional
526 targets lst-1 and sygl-1. PLoS Genet 16, e1008650.
527
528 Crittenden, S.L., Lee, C., Mohanty, I., Battula, S., Knobel, K., Kimble, J., 2019. Sexual dimorphism
529 of niche architecture and regulation of the Caenorhabditis elegans germline stem cell pool. Mol
530 Biol Cell 30, 1757-1769.
531
532 Dalfo, D., Ding, Y., Liang, Q., Fong, A., Cipriani, P.G., Piano, F., Zheng, J.C., Qin, Z., Hubbard,
533 E.J.A., 2020. A Genome-Wide RNAi Screen for Enhancers of a Germline Tumor Phenotype
534 Caused by Elevated GLP-1/Notch Signaling in Caenorhabditis elegans. G3 (Bethesda) 10, 4323-
535 4334.
536
537 Dejima, K., Hori, S., Iwata, S., Suehiro, Y., Yoshina, S., Motohashi, T., Mitani, S., 2018. An
538 Aneuploidy-Free and Structurally Defined Balancer Chromosome Toolkit for Caenorhabditis
539 elegans. Cell Rep 22, 232-241.
540
541 Dickinson, D.J., Ward, J.D., Reiner, D.J., Goldstein, B., 2013. Engineering the Caenorhabditis
542 elegans genome using Cas9-triggered homologous recombination. Nat Methods 10, 1028-1034.
543
544 Gordon, K.L., Zussman, J.W., Li, X., Miller, C., Sherwood, D.R., 2020. Stem cell niche exit in C.
545 elegans via orientation and segregation of daughter cells by a cryptic cell outside the niche. Elife
546 9.
547 Govindan, J.A., Nadarajan, S., Kim, S., Starich, T.A., Greenstein, D., 2009. Somatic cAMP
548 signaling regulates MSP-dependent oocyte growth and meiotic maturation in C. elegans.
549 Development 136, 2211-2221.

Hall, D.H., Winfrey, V.P., Blaeuer, G., Hoffman, L.H., Furuta, T., Rose, K.L., Hobert, O., Greenstein, D., 1999. Ultrastructural features of the adult hermaphrodite gonad of Caenorhabditis elegans: relations between the germ line and soma. Dev Biol 212, 101-123.

Henderson, S.T., Gao, D., Lambie, E.J., Kimble, J., 1994. lag-2 may encode a signaling ligand for the GLP-1 and LIN-12 receptors of C. elegans. Development 120, 2913-2924.

Huang, L.S., Sternberg, P.W., 1995. Genetic dissection of developmental pathways. Methods Cell Biol 48, 97-122.

Hubbard, E.J., Greenstein, D., 2000. The Caenorhabditis elegans gonad: a test tube for cell and developmental biology. Dev Dyn 218, 2-22.

Hubbard, E.J.A., Schedl, T., 2019. Biology of the Caenorhabditis elegans Germline Stem Cell System. Genetics 213, 1145-1188.

Kershner, A.M., Shin, H., Hansen, T.J., Kimble, J., 2014. Discovery of two GLP-1/Notch target genes that account for the role of GLP-1/Notch signaling in stem cell maintenance. Proceedings of the National Academy of Sciences.

Killian, D.J., Hubbard, E.J., 2005. Caenorhabditis elegans germline patterning requires coordinated development of the somatic gonadal sheath and the germ line. Dev Biol 279, 322-335.

Kocsisova, Z., Kornfeld, K., Schedl, T., 2019. Rapid population-wide declines in stem cell number and activity during reproductive aging in C. elegans. Development 146.

578 Lee, C., Shin, H., Kimble, J., 2019. Dynamics of Notch-Dependent Transcriptional Bursting in Its
579 Native Context. Dev Cell 50, 426-435 e424.
580
581 Lee, C., Sorensen, E.B., Lynch, T.R., Kimble, J., 2016. C. elegans GLP-1/Notch activates
582 transcription in a probability gradient across the germline stem cell pool. eLife 5.
583
584 McCarter, J., Bartlett, B., Dang, T., Schedl, T., 1997. Soma-germ cell interactions in
585 Caenorhabditis elegans: multiple events of hermaphrodite germline development require the
586 somatic sheath and spermathecal lineages. Developmental Biology 181, 121-143.
587
588 Miyata, S., Begun, J., Troemel, E.R., Ausubel, F.M., 2008. DAF-16-dependent suppression of
589 immunity during reproduction in Caenorhabditis elegans. Genetics 178, 903-918.
590
591 Mohammad, A., Vanden Broek, K., Wang, C., Daryabeigi, A., Jantsch, V., Hansen, D., Schedl, T.,
592 2018. Initiation of Meiotic Development Is Controlled by Three Post-transcriptional Pathways in
593 Caenorhabditis elegans. Genetics 209, 1197-1224.
594
595 Nadarajan, S., Govindan, J.A., McGovern, M., Hubbard, E.J., Greenstein, D., 2009. MSP and GLP-
596 1/Notch signaling coordinately regulate actomyosin-dependent cytoplasmic streaming and
597 oocyte growth in C. elegans. Development 136, 2223-2234.
598
599 Oshima, A., Tani, K., Fujiyoshi, Y., 2016. Atomic structure of the innexin-6 gap junction channel
600 determined by cryo-EM. Nat Commun 7, 13681.
601
602 Pekar, O., Ow, M.C., Hui, K.Y., Noyes, M.B., Hall, S.E., Hubbard, E.J.A., 2017. Linking the
603 environment, DAF-7/TGFbeta signaling and LAG-2/DSL ligand expression in the germline stem
604 cell niche. Development 144, 2896-2906.
605

606 Penkner, A.M., Fridkin, A., Gloggnitzer, J., Baudrimont, A., Machacek, T., Woglar, A., Csaszar, E.,
607 Pasierbek, P., Ammerer, G., Gruenbaum, Y., Jantsch, V., 2009. Meiotic chromosome homology
608 search involves modifications of the nuclear envelope protein Matefin/SUN-1. Cell 139, 920-
609 933.
610
611 Phelan, P., 2005. Innexins: members of an evolutionarily conserved family of gap-junction
612 proteins. Biochim Biophys Acta 1711, 225-245.
613
614 Shin, H., Haupt, K.A., Kershner, A.M., Kroll-Conner, P., Wickens, M., Kimble, J., 2017. SYGL-1 and
615 LST-1 link niche signaling to PUF RNA repression for stem cell maintenance in Caenorhabditis
616 elegans. PLoS Genet 13, e1007121.
617
618 Skerrett, I.M., Williams, J.B., 2017. A structural and functional comparison of gap junction
619 channels composed of connexins and innexins. Dev Neurobiol 77, 522-547.
620
621 Starich, T., Greenstein, D., 2020. A Limited and Diverse Set of Suppressor Mutations Restore
622 Function to INX-8 Mutant Hemichannels in the Caenorhabditis elegans Somatic Gonad.
623 Biomolecules 10.
624
625 Starich, T.A., Bai, X., Greenstein, D., 2020. Gap junctions deliver malonyl-CoA from soma to
626 germline to support embryogenesis in Caenorhabditis elegans. Elife 9.
627
628 Starich, T.A., Hall, D.H., Greenstein, D., 2014. Two classes of gap junction channels mediate
629 soma-germline interactions essential for germline proliferation and gametogenesis in
630 Caenorhabditis elegans. Genetics 198, 1127-1153.
631
632 Yochem, J., Greenwald, I., 1989. glp-1 and lin-12, genes implicated in distinct cell-cell
633 interactions in C. elegans, encode similar transmembrane proteins. Cell 58, 553-563.
634

635 Zhou, Z., Hartwieg, E., Horvitz, H.R., 2001. CED-1 is a transmembrane receptor that mediates
636 cell corpse engulfment in C. elegans. Cell 104, 43-56.

637

638

639 **Materials and Methods**

640

641 *Live imaging and image analysis of live samples*

642

643 Live specimens were grown at 20°C, and staged by picking mid-L4 larvae, then allowing them to
644 grow at 20°C until imaging them 24 hours later. Animals were immobilized using 10mM
645 Levamisole (Sigma T1512) in M9 buffer. Imaging was carried out on a Nikon W1 spinning disk
646 confocal microscope.

647

648 Image analysis was carried out on 2-dimensional maximum-projection Z-stack images of 3D
649 confocal data. The distance from the distal end of the gonad to the end of each DTC process
650 was measured along a line drawn from the end of each process parallel to the distal-proximal
651 axis to a line drawn tangent to the distal end, orthogonal to the distal-proximal axis line (Figure
652 1—figure supplement 1). The distance between the distal end of the gonad and the most distal
653 extent of Sh1 was measured in the same way. All data points were recorded for each sample
654 and used to calculate the mean values presented in Figures 1 and 2.

655

656 Sh1 visualization in live worms: *bcIs39* [*lim-7p*::CED-1::GFP] (Zhou et al., 2001) encodes a
657 functional membrane-localized fusion to CED-1. *tnIs5* and *tnIs6* encode an identical non-
658 functional fusion to the first 61 amino acids of LIM-7 (*tnIs5* or *tnIs6*) denoted here as "*lim-*
659 *7p*::GFP" that includes 2.23kb upstream, the first two exons, and the first intron of *lim-7* fused
660 to GFP (Hall et al., 1999).

661

DTC visualization in live worms: *naIs37* [*lag-2p*::mCherry-PH] encodes mCherry fused to the PH domain of rat phospholipase C delta (Pekar et al., 2017) and *qIs154* [*lag-2p*::MYR-tdTomato] encodes a src kinase myristoylation sequence fused to tdTomato (Byrd et al., 2014).

Strains

C. elegans strains (Table S1) were grown on standard NGM media [containing 6.25 mg/ml Nystatin (added after autoclaving) and 200 mg/ml streptomycin sulphate (added before autoclaving)] with *E. coli* strain OP50-1 as food source. Similar results were obtained on NGM medium with OP50 as food source and without inclusion of streptomycin sulphate in the media. Strains were grown at 20°C. In addition to the wild-type strain N2, the following alleles, described in WormBase (www.wormbase.org) or in the cited references, were used:

Chr. I—*inx-14(ag17)* (Miyata et al., 2008; Starich et al., 2014), *sygl-1(q983[3xOLLAS::sygl-1])* (Shin et al., 2017) .

Chr. IV—*inx-8(qy78[mKate2::inx-8])* (Gordon et al., 2020) , *inx-8(qy78 tn2031)* (this work), *inx-8(tn2034)* (this work), *inx-9(ok1502), inx-8(qy102[mKate2::inx-8)] inx-9(ok1502)* (Gordon et al., 2020), *inx-8(tn1513tn1553) inx-9(ok1502)* (Starich and Greenstein, 2020), *inx-8(tn1513tn1555) inx-9(ok1502)* (Starich et al., 2020).

Balancer chromosomes (Dejima et al., 2018) used included: *tmC18 [dpy-5(tmIs1236)]* I, *tmC27[tmIs1239]* I, *tmC5[tmIs1220]* IV.

Integrated transgenes included: *mIs11[myo-2p::gfp + pes-10p::gfp + gut promoter::gfp]* IV, *bcIs39[lim-7p::ced-1::gfp + lin-15(+)]* V (Zhou *et al*., 2001), *qIs154[lag-2p::MYR::tdTomato +ttx-3p::gfp]* V (Byrd et al., 2014) , *tnIs5[lim-7p::gfp + rol-6(su1006)]* X*, tnIs6[lim-7p::gfp + rol-6(su1006)]* X (Hall et al., 1999) , *cpIs122[lag-2p::mNeonGreen::plcdeltaPH]* (Gordon et al., 2020), *naIs37[lag-2p::mCherry:: plcdeltaPH + unc-119(+)]* (Pekar et al., 2017).

Extrachromosomal arrays used included: *tnEx42[acy-4::gfp + rol-6(su1006)]* (Govindan et al., 2009).

Table S1. Strains used in this study

Strain	Genotype	Reference
DG4959	*qIs154 V; tnIs5 X*	(this work)
DG4977	*inx-14(ag17) I; qIs154 V; tnIs5 X*	(this work)
DG5020	*bcIs39 V; naIs37*	(this work)
DG5026	*inx-14(ag17) I; bcIs39 V naIs37*	(this work)
DG5027	*inx-9(ok1502) IV; bcIs39 V; naIs37*	(this work)
DG5029	*inx-8(tn1513 tn1555) inx-9(ok1502) IV; bcIs39 V; naIs37*	(this work)
DG5059	*inx-9(ok1502) IV*	(this work)
DG5063	*inx-8(qy78) IV*	(this work)
DG5064	*inx-8(qy102) inx-9(ok1502) IV*	(this work)
DG5070	*inx-14(ag17) I; inx-8(qy78) IV*	(this work)
DG5131	*inx-8(qy78) IV; bcIs39 V; naIs37*	(this work)
DG5133	*inx-8(qy102) inx-9(ok1502) IV; bcIs39 V; naIs37*	(this work)
DG5136	*sygl-1(q983) I; bcIs39 V; naIs37*	(this work)
DG5150	*inx-14(ag17) sygl-1(q983) I; bcIs39 V; naIs37*	(this work)
DG5181	*sygl-1(q983) I; inx-8(qy78) IV; bcIs39 V; naIs37*	(this work)
DG5229	*inx-8(qy78 tn2031) IV; bcIs39 V; naIs37*	(this work)
DG5232	*inx-8(tn2034) IV; bcIs39 V; naIs37*	(this work)
DG5248	*sygl-1(q983) I; inx-8(qy78 tn2031) IV; bcIs39 V; naIs37*	(this work)
DG5249	*sygl-1(q983) I; inx-8(tn2034) IV; bcIs39 V; naIs37*	(this work)
DG5250	*inx-8(qy78 tn2031) IV*	(this work)
DG5251	*inx-8(tn2034) IV*	(this work)
DG5270	*inx-14(ag17) I*	(this work)
KLG006	*inx-8(qy78) IV; tnIs6 X; cpIs122*	(Gordon et al., 2020)

Strain constructions

Multiply mutant strains were constructed in a straightforward manner (Huang and Sternberg, 1995). *tmC18* was used as a balancer chromosome for *inx-14(ag17)*. *tmC27* was used as a balancer chromosome for *sygl-1(q983)*. *tmC5* or *mIs11* were used as balancer chromosomes for *inx-8* and *inx-9* mutant alleles. The presence of *inx-14(ag17)* in strains was verified by PCR and DNA sequencing. The *ag17* allele was originally described as an Arg to His change in the second extracellular loop of INX-14, but the exact residue position was not specified (Miyata et al., 2008). A 1.2-kb PCR fragment covering this region was amplified with primers inx-14delF and inx-14delR (see Table S1 for the sequence of oligonucleotides used in this study). The PCR fragment was sequenced with the inx-14delR primer. No sequence changes were found in Arg residues predicted to occupy the second extracellular loop. However, a CGT to CAT (R326H) change was identified at a residue position predicted to lie near the cytoplasmic end of the fourth transmembrane domain, and we surmise that this change represents the original *ag17* mutation. The presence of the *sygl-1(q983[3xOLLAS::sygl-1])* mutation in strains was verified by PCR with primers sygl1-F and sygl1-R, which produce a 216 bp product in the wild type and a 348 bp product in *sygl-1(q983)* and by anti-OLLAS staining. The presence of *inx-8(qy78 tn2031)* and *inx-8(tn2034)* in strains was verified by PCR with oligonucleotide primers inx8_delta.F and inx8_delta.R.

Brood counts and Embryonic lethality measurements

L4-stage hermaphrodites were cultured individually and transferred approximately every 24 hours until they stopped producing embryos (4–6 days). Worms that crawled off the media and died were redacted (varied from 0–10% depending on the experiment). Embryos that failed to hatch after 24–36 hours were counted and scored as dead. In the majority of cases, these embryos exhibited morphological abnormalities. Control experiments demonstrated that these embryos were not simply delayed and never hatched. Embryos that hatched were counted and scored as viable. This includes embryos in *inx-8(qy78)* that died shortly after hatching, arrested as larvae, and/or exhibited morphological abnormalities.

749

750 *Genome editing*

751

752 CRISPR-Cas9 genome editing was used to generate *inx-8* null alleles in both the *inx-*
753 *8(qy78[mKate2::inx-8])* and wild-type genetic backgrounds. The approach taken generated
754 identical 1524 bp deletions within the *inx-8* locus in both genetic backgrounds starting 136 bp
755 upstream of the wild-type inx-8 ATG start codon and extending 221 bp into *inx-8* exon 3. In the
756 *inx-8(qy78[mKate2::inx-8])* context, this edit removes both the mKate2 moiety and *inx-8*. The
757 deletions are expected to constitute *inx-8* null alleles because, in addition to removing the start
758 codon, they delete amino acids 1–349 (out of 382 amino acids), including virtually all residues
759 essential for spanning the plasma membrane and forming a channel (Starich and Greenstein,
760 2020). The approach used pRB1017 to express two single guide RNAs (sgRNAs) under control of
761 the C. elegans U6 promoter (Arribere et al., 2014). Oligonucleotides inx8_us_sgRNA1.F and
762 inx8_us_sgRNA1.R were annealed and used to generate the plasmid inx8_us_sgRNA1 to direct
763 Cas9 cleavage 136 bp upstream of the ATG initiator codon (Table S1 lists the sequences of all
764 oligonucleotides used in this study). Oligonucleotides inx8_sgRNA1.F and inx8_sgRNA1.R were
765 annealed and used to generate the plasmid inx8_sgRNA1 to direct Cas9 cleavage in exon 3. To
766 generate sgRNA clones, annealed oligonucleotides were ligated to BsaI-digested pRB1017
767 plasmid vector, and the resulting plasmids were verified by Sanger sequencing. pDD162 served
768 as the source of Cas9 expressed under control of the *eef-1A.1/eft-3* promoter (Dickinson et al.,
769 2013). The repair template oligonucleotide used was inx8_rpr. Genome editing employed the
770 dpy-10 co-conversion method (Arribere et al., 2014). The injection mix contained pJA58 (7.5
771 ng/µl), AF-ZF-827 (500 nM), inx8_us sgRNA1 (25 ng/µl), inx8_sgRNA1 (25 ng/µl), inx8_rpr (500
772 nM), and pDD162 (50 ng/µl) and was injected into adult hermaphrodites from strains DG5131
773 *inx-8(qy78[mKate2::inx-8]) IV; bcIs39[lim-7p::ced-1::gfp + lin-15(+)] V; naIs37[lag-*
774 *2p::mCherry::PH + unc-119(+)]* and DG5020 *bcIs39[lim-7p::ced-1::gfp + lin-15(+)]V; naIs37[plag-*
775 *2::mCherryPH + unc-119(+)]*. Correct targeting was verified by conducting PCR with primer pairs
776 inx8_delta.F and inx8_delta.R followed by DNA sequencing. Three deletion alleles were
777 recovered from the injections into DG5131 *(qy78tn2031, qy78tn2032,* and *qy78tn2033)*, and

two deletion alleles were recovered from the injections into DG5020 *(tn2034* and *tn2035)*. The deletion alleles were outcrossed to *tmC5(tmIs1220[pmyo-2::Venus])/+ IV; bcIs39[lim-7p::ced-1::gfp + lin-15(+)/+V; naIs37[plag-2::mCherryPH + unc-119(+)]/+* males. Homozygous strains were analyzed by confocal microscopy.

Table S2. Oligonucleotides used in this study

Oligo name	Sequence
inx8_us_sgRNA1.F	TCTTGTGGAAAACAGAGGAATGGG
inx8_us_sgRNA1.R	AAACCCCATTCCTCTGTTTTCCAC
inx8_sgRNA1.F	TCTTGAGTGACTTGGTAGCATCGG
inx8_sgRNA1.R	AAACCCGATGCTACCAAGTCACTC
inx8_RPR	GGTGGCCAATAAAAATGCTTTTCTTTTTGCTTTT CTCTATCTACTTCCGTTCCGCCCCGGAGGTTGCC GTGGAGATGTACAGCGACTTTTTAGTAAGTCTTT TCAAC
inx8_delta.F	CCTTCGACCTGATTTCCCCTTCTTCTAATG
inx8_delta.R	CTATTGCTTTCCGTTCTTCAAGATGTTGTTG

Immunostaining and image analysis of fixed samples

Immunostaining was carried out as described (Mohammad et al., 2018). Briefly, synchronized adult hermaphrodites, 24-hr past mid-L4, were dissected in PBST (PBS with 0.1% Tween 20), with 0.2 mM levamisole to extrude the gonads. The gonads were fixed in 3% paraformaldehyde solution for 10 min and then post-fixed in −20° chilled methanol for 10 min. After 3x 10-min washes with PBST, they were blocked in 30% goat serum for 30 min at RT. The gonads were then incubated with the desired primary antibodies diluted (see below) in 30% goat serum at 4° overnight. The next day, after 3x 10-min PBST washes, the gonads were further incubated with appropriate secondary antibodies, diluted in 30% goat serum, at 4° overnight. The gonads were washed 3 times with PBST, then incubated with 0.1 g/ml DAPI in PBST for 30 min. After removal

of excess liquid, the gonads were mixed with anti-fading agent (Vectashield) and transferred to an agarose pad on a slide. Hyperstack images were captured using a spinning disk confocal microscope (PerkinElmer-Cetus, Norwalk, CT). Two overlapping hyperstack images were captured for each gonad arm to obtain coverage of >50 cell diameters from the distal end of the gonad. Images were further processed in Fiji, and DAPI stained nuclei were used to mark the number of cell diameters from the distal end. Employing pixel to micron ratio, specific to the images captured, cell diameters were converted into microns where required.

SYGL-1 zone length assessment: OLLAS staining was used to assess 3xOLLAS::SYGL-1 accumulation (Shin et al., 2017). In wild-type young adults, SYGL-1 accumulates at the distal end of the germline and is downregulated around 10 cell diameters from the distal tip (Kocsisova et al., 2019; Shin et al., 2017). Cell diameters were counted from the distal end of the germline up to the row where SYGL-1 is no longer visible by eye. OLLAS staining in the wild type worms without OLLAS tag was used to differentiate staining from the background. To confirm the accuracy of our visual assessment, we quantified the intensity of SYGL-1 accumulation in the distal germline, employing methods similar to Chen et al., 2020 in the same set of germlines where the SYGL-1 zone was visually evaluated. We found that the cell diameter position called as the end of the SYGL-1 zone consistently corresponded to 6 – 9% of peak SYGL-1 intensity, for each genotype. These results indicate that the SYGL-1 zone length visual assessment was reproducible and consistent.

Progenitor zone length assessment: The gonads were stained with a progenitor zone marker, CYE-1, and an early meiotic prophase marker, pSUN-1, (anti-SUN-1 S8-Pi) (Mohammad et al., 2018). For assessing the progenitor zone length, cell diameters (rows) were counted from the distal end of the germline, where all cells are CYE-1 positive, till the point after which the majority of the cells in a row have switched from staining for CYE-1 to pSUN-1. Note that pSUN-1 staining is not shown in the figures though it was used to assess the PZ border.

Assessment of distal position of Sh1: anti-GFP antibody staining was used to visualize the sheath, where cell diameters were counted from distal end to the point where GFP staining became prominent.

Primary antibodies used: mouse anti-CYE-1 (1:100; (Brodigan et al., 2003)); guinea pig anti-SUN-1 S8-Pi (1:1000; (Penkner et al., 2009)); rat anti-OLLAS (1:2000; Novus Biological); rabbit anti-GFP (1:200; from Swathi Arur, MD Anderson Cancer Center).

Secondary antibodies used: Alexa Fluor 647 goat anti-mouse (Life Technologies), Alexa Fluor 594 goat anti-guinea pig (Invitrogen), Alexa Fluor 594 donkey anti-rat (Invitrogen), Alexa Fluor 488 goat anti-rabbit (Invitrogen).

Funding

ACS grant PF-19-231-01-CSM to TT

NIH R35GM134876 and R01AG065672 to EJAH

R01 GM100756 to T. Schedl

NIH GM57173 to DG

Contributions

TT, EJAH, wrote the manuscript with contributions from all authors.

TT, AM, DG, T Starich performed analyzed and interpreted experiments.

EJAH, T Schedl, DG oversaw experiments and analysis

Competing interests

E.J.A.H. holds US patent 6,087,153.

865